Smooth polar caps for locally quad-dominant meshes

Kęstutis Karčiauskas[a], Jörg Peters[b,*]

[a] *Vilnius University, Lithuania*
[b] *University of Florida, USA*

Abstract

A polar configuration is a node surrounded by m triangles. Polar configurations are common to cap off cylinders and spheres. When the triangles, interpreted as quadrilaterals with one edge collapsed, are surrounded by a quad-strip then the extended polar configuration qualifies as a part of *locally quad-dominant* (lqd) mesh. Recent constructions, referred to as semi-structured splines, can use lqd meshes as control nets: multi-sided configurations that merge parameter directions are covered by G-spline; and T-junctions that transition from coarse and fine are covered by GT-splines.

This paper complements existing semi-structured splines by providing the missing component for polar configurations. A spectrum of constructions of differing degree are introduced, tested and compared. Bi-2 C^1 splines are extended to polar configurations covered by C^1 surfaces consisting of (macro-)patches of degree as low as bi-2. Bi-3 C^2 splines are extended to polar configurations covered by surfaces that are C^2 except for a C^1 pole and consist of (macro-)patches of degree as low as bi-3.

Keywords: polar configuration, generalized spline surface, locally quad-dominant, semi-structured

1. Introduction

Polar meshes, where a cylindrical structure is closed off, occur naturally in the modeling of air plane nose cones, finger tips and similar protrusions. Modeling such tips as the common corner of a large number of surrounding quadrilaterals yields a jagged star-pattern that most surface constructions fail to convert into a well-shaped smooth surface: the problem is a lack of alignment of the jagged path with the smooth circular cylinder direction. Polar meshes are therefore better modelled by explicitly acknowledging the singularity of the tip. Coalescing the top edges of a cylindrical mesh into one point, the pole, yields a *polar configuration*: m quadrilaterals, one of whose edges is collapsed into the pole, while the opposing edge is aligned with the circular direction as in Fig. 1a.

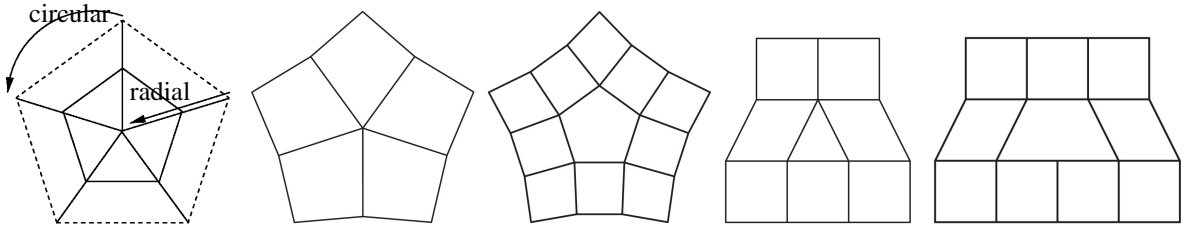

(a) polar-net $m = 5$ (b) star-net $n = 5$ (c) n-gon-net, $n = 5$ (d) τ_0-net (e) τ_1-net

Figure 1: Locally quad-dominant (lqd) mesh patterns. Our focus is on (a) and combinations with the other patterns. (The pentagon in (e) is called a T_1-gon, the triangle in (d) is called a T_0-gon; a T-gon with correct valencies and surrounded by quadrilaterals is called τ-net.)

*Corresponding author
Email addresses: kestutis.karciauskas@mif.vu.lt (Kęstutis Karčiauskas), jorg.peters@gmail.com (Jörg Peters)

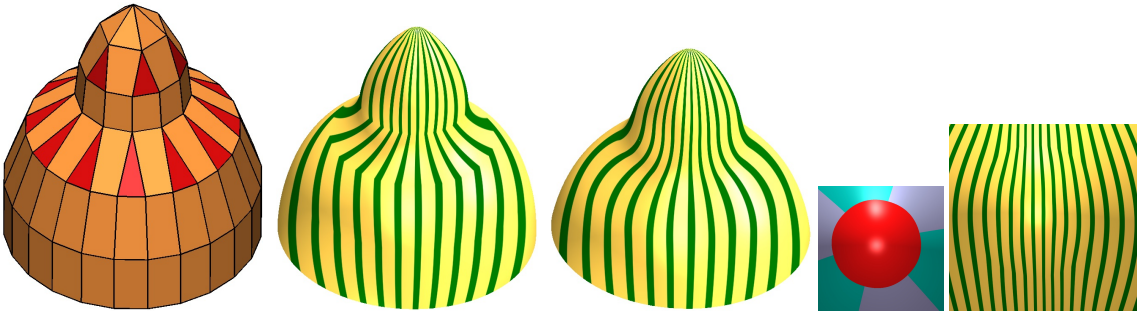

(a) input mesh (b) bi-2 polar (c) bi-3 polar

Figure 2: Mesh with τ_0-configurations completed by a polar configuration of valence 6. (a) If we interpret the polar cone's triangles as degenerate quads, each triangular T_0-gon facet is surrounded by quads forming a τ_0-configuration. (b) highlight line distribution when interpreting the regular input as a bi-2 spline net, and applying the polar construction of Section 4 and Karčiauskas and Peters (2019b). (c) highlight line distribution when interpreting the regular input as a C^2 bi-3 spline net and applying the polar construction of Section 5 and Karčiauskas and Peters (2019a).

Two classes of surface constructions can use polar configurations as control nets: polar subdivision surfaces and polar splines (see Section 1.1). Polar subdivision can achieve good shape but produces an infinite sequence of nested rings. This work therefore focuses on polar splines. Polar splines extend tensor-product splines and complement recent constructions that we jointly refer to as semi-structured splines. Such semi-structured splines can use as control nets a *locally quad-dominant* (lqd) mesh, i.e. a mesh where all non-4-sided facets are surrounded by quadrilaterals. Multi-sided star-configurations or polyhedral cells (see Fig. 1b,c) are covered by smooth G-splines that merge parameter directions, and τ-configurations (Fig. 1d,e) bridge between coarse and fine meshes and are covered by GT-splines. Polar splines use as control net any polar configuration. Polar configurations fit the lqd definition when the triangles are interpreted as degenerate quadrilaterals with one edge collapsed.

The new polar spline of degree bi-3, matches the degree of the regular surface regions, and is C^2 except at central point where it is C^1. It has as good a highlight line distribution as C^2 constructions of twice the degree and so demonstrates that formal C^2 smoothness is not necessary for good shape. The top of Fig. 2a shows a typical *polar configuration* of valence $n = 6$ consisting of six triangles with a common vertex. An analogous smooth polar construction for capping bi-2 regular regions uses patches of degree bi-2.

The new polar constructions

- cap polar configurations with good highlight line distribution;
- the pole's direct neighbors can be $n \neq 4$-valent nodes or nodes of T-gons (tight configurations);
- are of low polynomial degree (bi-2, bi-3);
- and so complement
  - regular (bi-2 C^1, bi-3 C^2) tensor-product splines;
  - GT-constructions;
  - multi-sided G-spline constructions;
- are refinable and suitable as finite elements for engineering analysis.

Overview After reviewing the literature of constructions for polar configurations, in Section 1.1, Section 2 introduces the notation and setup and summarizes recent semi-structured splines. The constructions use a reparameterization defined in Section 3. Section 4 and Section 5 then present the bi-2, respectively bi-3 capping polar splines.

1.1. Review of polar constructions

Applying the popular subdivision Catmull and Clark (1978) to extend C^2 bi-3 splines to a polar mesh yields poor highlight line distributions as illustrated in Fig. 3c. The same holds for Doo-Sabin subdivision extending C^1 bi-2 splines, see Fig. 10a. Both surface constructions suffer from mis-alignment with the natural circular direction. Point-augmented bi-2 C^1 subdivision surfaces Karčiauskas and Peters (2015a) improves the shape of Doo-Sabin

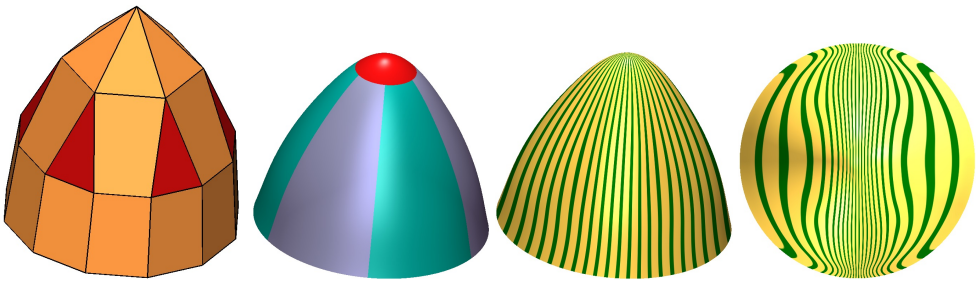

(a) input (b) base of Karčiauskas and Peters (2019a) + red polar cap

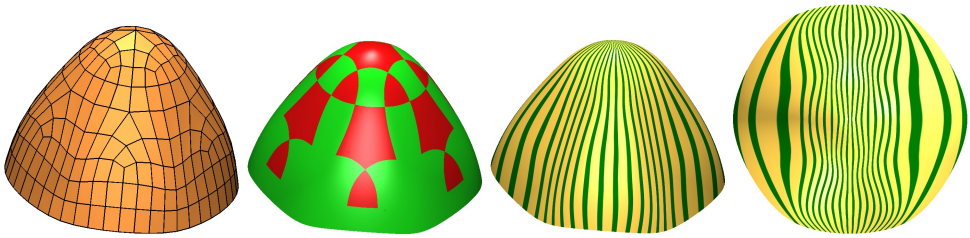

(c) Catmull-Clark: input = (a) twice subdivided

Figure 3: Comparison to Catmull-Clark subdivision. (a) T-gon mesh is the top of Fig. 2. (b) Covering the T_0-gons with Karčiauskas and Peters (2019a). (The hourglass highlight line pattern outside the parallel pattern of the polar configuration is due to this T_0-spline.) and the pole with the new bi-3 construction of Section 5 (c) Covering the T_0-gons with Catmull and Clark (1978) subdivision.

subdivision; and Bicubic Polar subdivision (B3PS) Karčiauskas and Peters (2007) improves the shape over Catmull-Clark. Both B3PS and Myles and Peters (2009) consist of contracting bi-3 rings that respect the natural circular direction and yield good highlight lines. The first is C^2 except at the limit point, where it is C^1, the second is everywhere C^2. Both Wang and Cheng (2013) and Myles and Peters (2009) illustrate a transition to polar layout via 5-valent vertices.

Karčiauskas and Peters (2009); Myles and Peters (2011); Shi et al. (2013); Wang and Cheng (2016); Toshniwal et al. (2017) derive a curvature continuous construction for polar configurations extending bi-3 splines by finitely many patches using the same approach. Toshniwal et al. (2017) differs somewhat by introducing a separate control structure at each pole to define the jet, an approach that was earlier used in Karčiauskas et al. (2006). Additionally Toshniwal et al. (2017) elaborate on the fact that the regular strips of the neighborhood of the polar cap can consist of tensor-product splines of differing degree. All polar and G-spline constructions can be used for engineering analysis Groisser and Peters (2015). Toshniwal et al. (2017) illustrate this point, emphasizing partition of 1. Wang and Cheng (2016) show how to interpolate the control net. The formally curvature continuous bi-3 extending polar constructions listed above are more complicated and require higher polynomial degree than the constructions presented in this paper.

Shi et al. (2010) take a different approach. The splines in a neighborhood are reparameterized in polar coordinates and then blended in the complex domain. This yields expo-rational surfaces that needs to be approximated by NURBS. Also transfinite constructions as in Várady et al. (2012) could be used to cover polar neighborhoods.

The polar construction of Karčiauskas and Peters (2009) is C^2 with good highlight line distribution. Each sector is a single patch, of degree 6 in the circular direction and degree 5 in the radial. Degree 6 is minimal for C^2 continuity at the pole where one edge of each patch collapses. However, formal C^2 continuity is not necessary for good highlight line distribution. The new construction's highlight line distribution is very close to that of the degree 6,5 C^2 construction; and it uses $2n$ bi-3 patches and a simpler algorithm than the $9n$ bi-3 patches also proposed in Karčiauskas and Peters (2009).

The new polar constructions complement semi-structured splines generalizing bi-3 splines Karčiauskas and Peters (2019a) and bi-2 splines Karčiauskas and Peters (2019b). Both are summarized in Section 2.

2. Definitions and Setup

All surfaces will be a collection of tensor-product patches in Bernstein-Bézier form (BB-form; see e.g. Farin (1988)):

$$\mathbf{f}(u,v) := \sum_{i=0}^{d_1}\sum_{j=0}^{d_2} \mathbf{f}_{ij} B_i^{d_1}(u) B_j^{d_2}(v)\ , \quad (u,v) \in [0..1]^2,$$

where $B_k^d(t) := \binom{d}{k}(1-t)^{d-k}t^k$ are the Bernstein polynomials of degree d and $\mathbf{f}_{ij} \in \mathbb{R}^3$ are the BB-coefficients (we will use bold face throughout for elements of $\mathbb{R}^3$). Connecting $\mathbf{f}_{ij}$ to $\mathbf{f}_{i+1,j}$ and $\mathbf{f}_{i,j+1}$ wherever possible yields the *BB-net*. For $i = 0, \ldots, d_1$, we index so that $\mathbf{f}_{i,d_2}$ are coalesced into one point, the pole, and refer to $\mathbf{f}_{i,j}$ as the jth *circular layer* and to $\mathbf{f}_{k,i}$ as the kth *radial layer*. Two tensor-product patches $\mathbf{f}^s$ and $\mathbf{f}^{s+1}$ sharing the pole join C^k then the curves formed by the jth circular layers join C^k for all j.

For any 3×3 grid in the mesh, the vertices can be interpreted as the control net of a bi-2 uniform B-spline. Expressing this spline in bi-2 BB-form is called *B-to-BB conversion*, see Fig. 4a. A partial conversion from a partial mesh yields a sub-net of the BB-net that defines position and first derivatives across an edge, see Fig. 4b. Analogously, a 4×4 grid in the mesh can be interpreted as the control net of a bi-3 uniform B-spline and partial conversion can define a BB-subnet that defines position, first and second derivatives across an edge (see Fig. 4c,d).

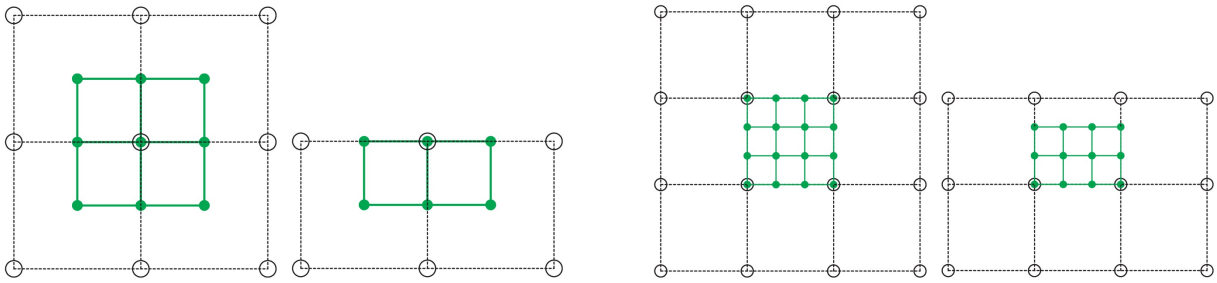

(a) bi-2 patch $\mathbf{p}$ (b) bi-2 tensor-border (c) bi-3 patch $\mathbf{p}$ (d) bi-3 tensor-border

Figure 4: (a,b) Bi-2 B-to-BB conversion. Circles ○ mark B-spline control points, solid disks ● mark BB-coefficients. The rules are: $\bullet_{\text{center}} = \circ_{\text{center}}$, $\bullet_{\text{edge}}$ = the average of $\circ_{\text{center}}$ and a neighbor ○, and $\bullet_{\text{corner}}$ = the average of the four surrounding ○. (c,d) Bi-3 B-to-BB conversion.

2.1. Some semi-structured splines

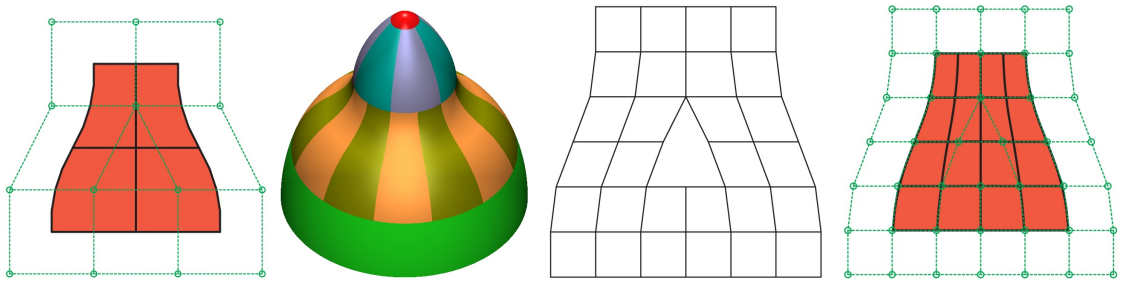

(a) τ_0-cap (b) surface (c) unifying net (d) GT(3)-spline

Figure 5: GT-spline constructions. (a) 4 pieces of a GT(2)-surface whose control net is the τ_0-net and (b) the surface combined with a polar cap. (c) The refined net unifying τ_0- and τ_1-input. (d) The 16 pieces of a GT(3)-surface derived from the unifying net.

A *star-configuration* with an extraordinary point is where more or less than four quads meet. Constructions, often abbreviated as G-splines, date back to the last millennium, e.g. Gregory and Hahn (1987), and modern constructions focus on generating good highlight line distributions, e.g. Loop and Schaefer (2008). A *T-junction* is where two facets

on one side meet one facet, the T-gon, on the other. A T_0-gon is a triangle as in Fig. 1d and a T_1-gon is formally a pentagon, with valences as in Fig. 1e. The lqd-submeshes enclosing them by quadrilaterals are called τ_0-nets and τ_1-nets. Most semi-structured splines are based on the concept of *geometric continuity*, i.e. smoothness after change of variables, see e.g. DeRose (1990). Patches $\mathbf{f}$ and $\hat{\mathbf{f}}$ that share a G-*edge* parameterized by $(u, 0 = v)$ are G^1 connected if they have matching derivatives after change of variables $\rho(u, v) := (u + b(u)v, a(u)v)$:

$$\partial_v \hat{\mathbf{f}}(u, 0) - a(u)\partial_v \mathbf{f}(u, 0) - b(u)\partial_u \mathbf{f}(u, 0) = 0\,. \tag{1}$$

The semi-structured splines in Karčiauskas and Peters (2019b), abbreviated GT(2) hereafter, extend first-order Hermite data defined by the τ-net. The data are obtained by interpreting the τ-net nodes as C^1 bi-2 B-spline control points and partially converting the Bernstein-Bézier (BB) form. This insures that the τ-cap smoothly joins the surrounding surface. In Fig. 5a the nodes of τ_0-net are displayed as $\circ$, the τ_0-cap consists of four C^1 connected pieces of degree $(2, 4)$ (2 in horizontal, 4 in vertical direction; an analogous τ_1-cap is build from 8 pieces of degree $(2, 4)$).

In Karčiauskas and Peters (2019a), semi-structured splines abbreviated GT(3) hereafter, are constructed treating the τ-nets as part of bi-3 C^2 spline mesh. Since bi-3 C^2 splines have a larger support then bi-2 splines, the τ-nets provide Hermite information only after a special refinement into a *unifying net*, displayed in Fig. 5c. Conversion of the unifying net yields second-order Hermite data in BB-form. In Fig. 5d the nodes of unifying net are displayed as $\circ$ and the spline consists of 16 pieces that are of degree 3 and C^2 in the horizontal direction. Unlike GT(2), the GT(3) construction offers various levels of continuity with the surrounding surfaces. G^2 continuity requires degree $(3, 9)$, G^1 continuity requires degree $(3, 5)$ and C^0 continuity requires degree $(3, 3)$, yet all achieve roughly the same highlight line distribution.

3. Polar reparameterizations ρ

C^1 continuity at the central point (pole) of polar cap requires reparameterizations ρ of the plane. We consider a regular planar m-gon (gray in Fig. 6a,b) with vertices

$$\mathbb{v}_i := \left[\begin{smallmatrix}\mathsf{c}_i\\ \mathsf{s}_i\end{smallmatrix}\right],\ i = 0, \ldots, m-1;\ \mathsf{c}_i := \cos\frac{2\pi\, i}{m}, \mathsf{s}_i := \sin\frac{2\pi\, i}{m}, \quad \text{and center } \mathbb{o} \in \mathbb{R}^2.$$

The ith piece $\rho^i : \mathbb{R}^2 \to \mathbb{R}^2$ of ρ covers the ith triangle of the m-gon and is of degree $(d, 1)$ where, depending on the context, $d = 2$ or $d = 3$. One layer of ρ^i is collapsed, i.e. $\rho^i_{j1} := \mathbb{o}$ for $j = 0, \ldots, d$, while its opposite interpolates vertices: $\rho^{i+1}_{00} := \mathbb{v}_{i+1} =: \rho^i_{d0}$ (see Fig. 6a,b).

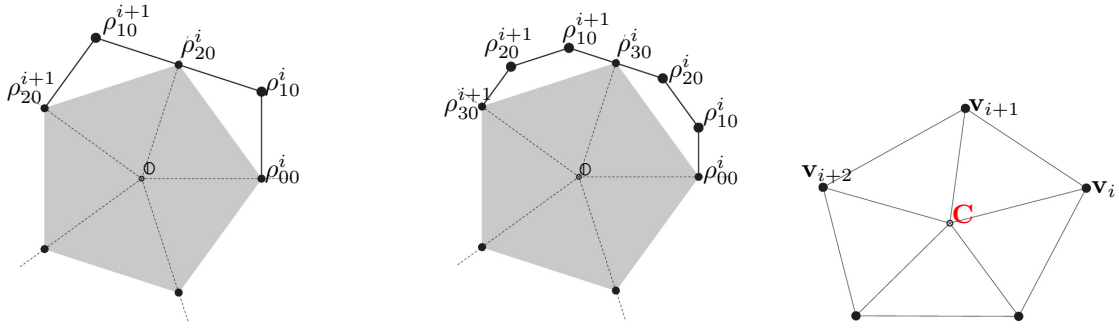

(a) ρ of degree (2,1) (b) ρ of degree (3,1) (c) linear map

Figure 6: Polar reparameterizations: (a) degree 2, (b) degree 3 with $\rho^i_{jk}, \mathbb{o}, \mathbb{v}_i \in \mathbb{R}^2$. (c) linear map with $\mathbf{C}, \mathbf{v}_i \in \mathbb{R}^3$.

For ρ of degree (2,1), it remains to define the BB-coefficients

$$\rho^i_{10} := \frac{\mathbb{v}_i + \mathbb{v}_{i+1}}{\mathsf{c}+1} + \frac{\mathsf{c}-1}{\mathsf{c}+1}\mathbb{o} \in \mathbb{R}^2, \text{ where } \mathsf{c} := \mathsf{c}_1. \tag{2}$$

By construction, adjacent pieces of ρ are C^1 connected.

For ρ of degree (3,1),

$$\rho^i_{10} := \frac{2\mathbb{v}_i + \mathbb{v}_{i+1}}{\mathsf{c}+2} + \frac{\mathsf{c}-1}{\mathsf{c}+2}\mathbb{o} \in \mathbb{R}^2, \qquad \rho^i_{20} := \frac{\mathbb{v}_i + 2\mathbb{v}_{i+1}}{\mathsf{c}+2} + \frac{\mathsf{c}-1}{\mathsf{c}+2}\mathbb{o} \in \mathbb{R}^2, \tag{3}$$

completes the definition. Then it is easily checked that adjacent pieces of ρ are C^2 connected.

Polar parameterized plane. To ensure existence of a unique normal at the pole $\mathbf{C}$, we define a linear map $\boldsymbol{\ell} : \mathbb{R}^2 \to \mathbb{R}^3$ piecemeal with each piece defined by coefficients $\mathbb{o}$, $\mathbf{v}_i$, $\mathbf{v}_{i+1}$ (see Fig. 6c) constrained so that

$$\mathbf{v}_{i+2} := -\mathbf{v}_i + 2\mathsf{c}\mathbf{v}_{i+1} + 2(1-\mathsf{c})\mathbf{C}. \tag{4}$$

Composing $\boldsymbol{\ell} \circ \rho$, the central point $\mathbf{C}$ is the image of origin $\mathbb{o}$, the points $\mathbf{v}_i$ are the images of the vertices v_i of the m-gon, and the other BB-coefficients of $\boldsymbol{\ell} \circ \rho$ are defined by (2), respectively (3) with v replaced by $\mathbf{v}$, $\mathbb{o}$ by $\mathbf{C}$ and $\mathbb{R}^2$ by $\mathbb{R}^3$. Variants of the expressions (2),(3) and (4) will appear in the polar constructions.

4. Polar capping of bi-quadratics

Given the often poor highlight line distribution of regular bi-2 C^1 tensor-product B-splines, the expectations for surfaces generalizing bi-2 splines to polar configurations can not be high. Nevertheless it is good to derive the bi-2 construction as it clarifies the principle ideas with simpler formulas than the bi-3 case. After the default construction of degree (2,3), this section presents a variant purely of degree bi-2, i.e. of minimal polynomial degree for C^1 continuity.

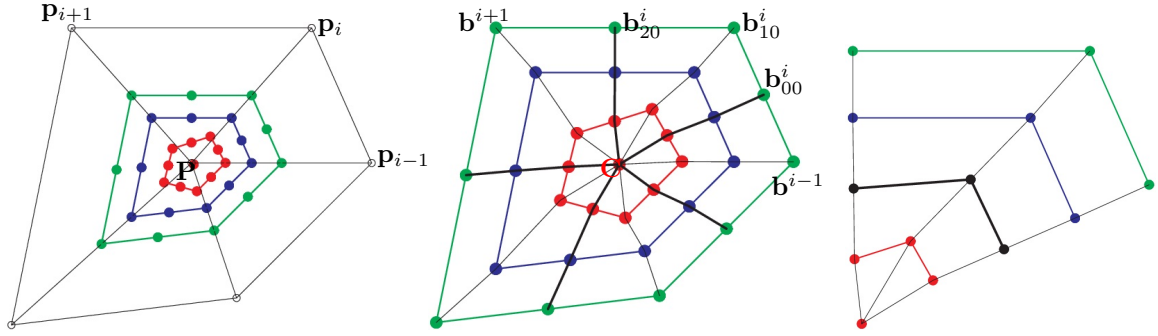

(a) polar net ⇒ BB-form (b) focus on the BB-net (c) bi-2 macropatch

Figure 7: Bi-degree $(2,3)$ construction and its transformation to a bi-2 macropatch.

First we construct a polar cap with a single patch per sector. Each patch is of degree $(2,3)$, degree 2 in the circular and degree 3 in the radial direction, see Fig. 7a,b. Fig. 7a shows a polar net with the vertices $\mathbf{p}_i$, $i = 0, \ldots, m-1$ and a central node (the pole) $\mathbf{P}$ of valence m. The triangles $\mathbf{p}_i\mathbf{p}_{i+1}\mathbf{P}$ are treated as the quads with one edge collapsed to $\mathbf{P}$.

The BB-form of the polar cap is displayed in Fig. 7b. The outermost circular layer of BB-coefficients $\mathbf{b}_{j0}$ are displayed as •, $\mathbf{b}_{j1}$ as •, $\mathbf{b}_{j2}$ as • and the innermost layer collapses to the pole $\mathbf{C}$:

$$\mathbf{b}^i_{j3} := \mathbf{C} := \frac{3}{4}\mathbf{P} + \frac{1}{4m}\sum_{i=0}^{m-1}\mathbf{p}_i,$$

Interpreting $\mathbf{p}_{i-1}$, $\mathbf{p}_i$, $\mathbf{P}$, $\mathbf{P}$ as four bi-2 B-spline control points, and applying the conversion of Section 2 yields the BB-coefficients of the quadratic boundary:

$$\mathbf{b}^i_{00} := \frac{1}{4}(\mathbf{p}_{i-1} + \mathbf{p}_i) + \frac{1}{2}\mathbf{P}, \quad \mathbf{b}^i_{10} := \frac{1}{2}\mathbf{p}_i + \frac{1}{2}\mathbf{P}, \quad \mathbf{b}^i_{20} := \frac{1}{4}(\mathbf{p}_i + \mathbf{p}_{i+1}) + \frac{1}{2}\mathbf{P}.$$

Setting $\mathbf{b}^i_{j1} := \frac{1}{3}\mathbf{P} + \frac{2}{3}\mathbf{b}^i_{j0}$, $j = 0, 1, 2$, connects the polar cap smoothly to any surrounding bi-2 B-spline surface. The formula for $\mathbf{b}^i_{02}$ insures that the points $\mathbf{b}^i_{02}$, $\mathbf{C}$ and $\mathbf{b}^i_{22}$ define a polar-parameterized plane and the parameterization then defines $\mathbf{b}^i_{12}$:

$$\mathbf{b}^i_{02} := \mathbf{C} + \frac{1}{3m}\sum_{s=0}^{m-1} \mathsf{c}_s \frac{1}{2}(\mathbf{p}_{i-1+s} + \mathbf{p}_{i+s}), \qquad \mathbf{b}^{i-1}_{22} := \mathbf{b}^i_{02}, \qquad \mathbf{b}^i_{12} := \frac{\mathbf{b}^i_{02} + \mathbf{b}^i_{22}}{\mathsf{c}+1} + \frac{\mathsf{c}-1}{\mathsf{c}+1}\mathbf{C}. \tag{5}$$

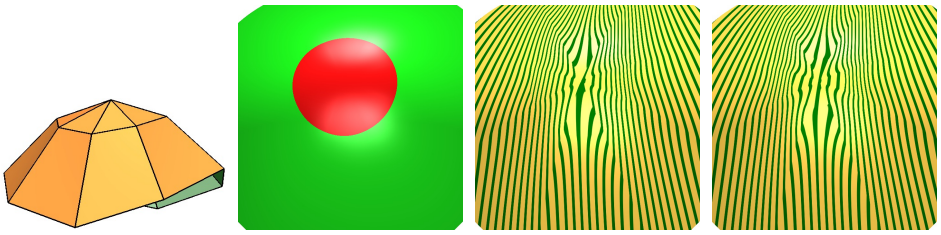

(a) net, $m = 8$ (b) layout (c) bi-23 (d) bi-2

Figure 8: Capping of extending bi-2 splines when the boundary is oscillating. Highlight lines on the surface generated from an extended convex polar net.

4.1. A two-piece bi-2 macropatch

To keep the overall degree minimal for C^1 continuity, each patch of degree (2,3) can be replaced by two C^1-joined patches of degree bi-2. Denoting the BB-coefficients of macropatch with the superscript $\boxminus$, (cf. Fig. 7b, Fig. 7c for the color code), the 2-piece bi-2 macropatch inherits first-order Hermite data both at the center and the outer boundary:

$$\bullet^{\boxminus} := \bullet, \quad \bullet^{\boxminus} := \frac{1}{4}\bullet + \frac{3}{4}\bullet, \qquad \mathbf{C}^{\boxminus} := \mathbf{C}, \quad \bullet^{\boxminus} := \frac{1}{4}\mathbf{C} + \frac{3}{4}\bullet, \tag{6}$$

hence is smoothly connected to surrounding surface; and $\bullet^{\boxminus} := \frac{1}{2}\bullet^{\boxminus} + \frac{1}{2}\bullet^{\boxminus}$ guarantees that the bi-2 macropatch polar cap is internally C^1.

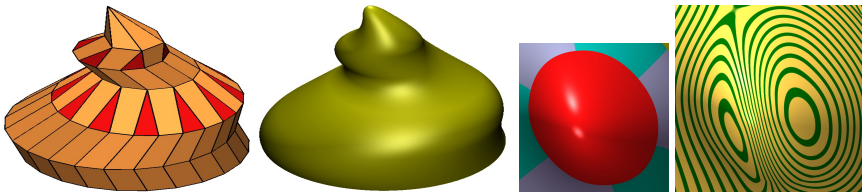

(a) cf. Fig. 2 (b) polar vicinity

Figure 9: Bi-2 generalizing capping of meshes with T_0-gons completed with a polar configuration whose boundary is close to planar.

4.2. Visual comparison of the bi-2 generalizing variants

This section takes a critical look at the low-degree options for C^1 polar caps. As pointed out earlier bi-2 C^1 tensor-product splines often have poor shape so that the expectations can not be high. Note that adding a regular layer around the polar configuration as in Fig. 8a yields a surrounding strip of regular bi-2 patches (green in Fig. 8b) for testing the quality of the transition to the polar cap. Fig. 8 and Fig. 9 show how oscillations in the input quad mesh affect low-degree polar caps. The highlight line distribution around the polar cap in Fig. 9 is considerably better than in Fig. 8. We traced the oscillations back to non-planarity of the circular parameter lines surrounding the polar cap and intentionally dislocated the surrounding quad layer in Fig. 8a to expose the differences in outcomes. Oscillations

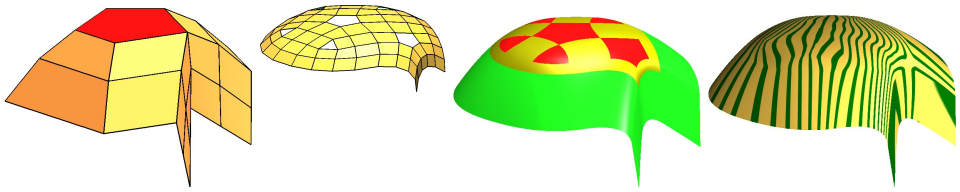

(a) Doo-Sabin subdivision

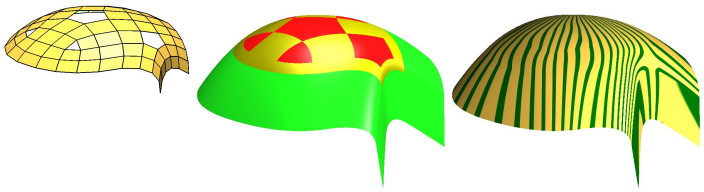

(b) finitely capped Augmented Subdivision

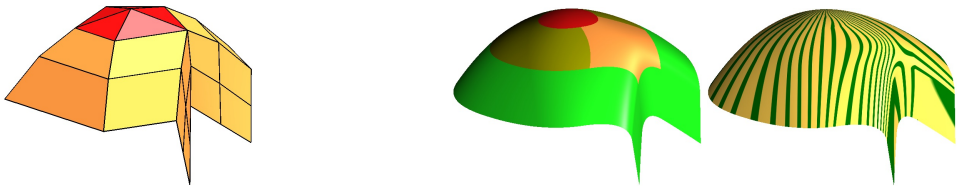

(c) new bi-2 polar + 6-sided bi-3 caps

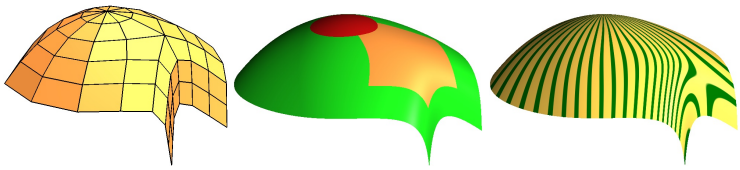

(d) new bi-3 polar on once-refined mesh of (c)

Figure 10: Comparison of bi-2 generalizing constructions. (a) input mesh, Doo-Sabin (DS) patch layout: bi-2 base, bi-2 two DS steps, DS subdivision surface. DS yield a flat top. (b) Augmented bi-2 Subdivision applied to the input mesh in (a), completed by degree bi-3 construction of Karčiauskas and Peters (2015b) improves on DS, but is more complicated than (c) where the polar construction is paired with the degree bi-3 construction. (d) The polar configuration is refined according to Section 5.1 and capped by the bi-3 C^2 generalizing polar construction of Section 5.

of the circular parameter lines near the pole can likely be avoided by a skilled designer but may occur in automated remeshing algorithms.

Fig. 10 compares subdivision and finite constructions. After two Doo-Sabin steps applied to the left input mesh, the middle-left submesh defines the yellow patches in Fig. 10a; continuing the Doo-Sabin refinement to visual completion yields the red caps. The undue flatness of the overall surface is the result of the first two steps. In Fig. 10b the first two steps are replaced by Augmented Subdivision Karčiauskas and Peters (2015b) and no flatness is observed when the surface is completed (red caps) by Augmented Subdivision. In Fig. 10c the polar node of the input mesh is chosen to be the central node of Augmented Subdivision, i.e.

$$\mu_n \bar{\mathbf{f}}_1 + (1-\mu_n)\bar{\mathbf{f}}_2 \text{ where } \mu_3 := 3/5 \text{ and } \mu_n := 2(n-2)/n \text{ for } n >= 4,$$

$\bar{\mathbf{f}}_1$ is the average of the pentagon vertices in (a), *left*, and $\bar{\mathbf{f}}_2$ is the average of these vertices' direct neighbors not on the pentagon. Now no refinement is needed. The C^2 bi-3 construction shown in Fig. 10d is explained in the next section. It yields the most uniform and rounded highlight line distribution.

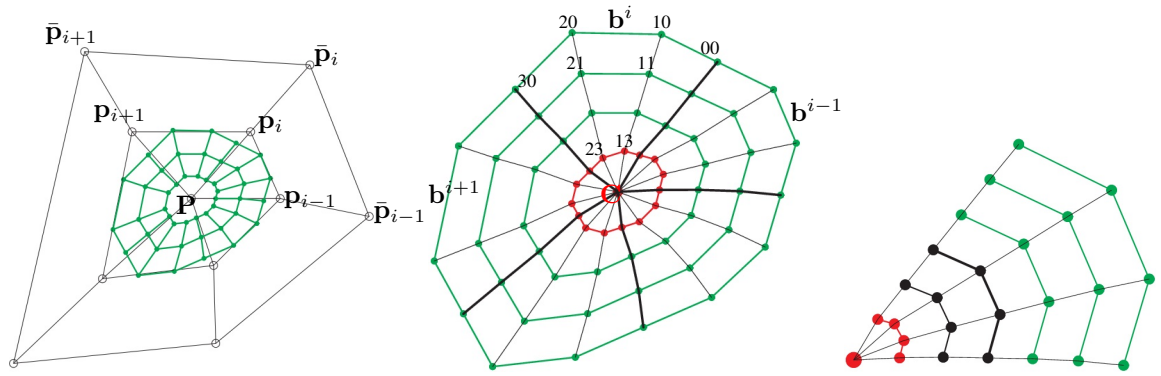

(a) polar net ⇒ BB-form (b) focus on the BB-net (c) bi-3 macropatch

Figure 11: Bi-degree $(3,4)$ construction and its transformation into a bi-3 macropatch.

5. Polar capping of bi-cubics

Analogous to Section 4, first a polar cap with a single patch per sector is constructed, this time of degree $(3,4)$. Fig. 11a shows a polar mesh with vertices $\bar{\mathbf{p}}_i$, $\mathbf{p}_i$, $i = 0,\dots,m-1$ and a central node, the pole $\mathbf{P}$ of valence m. Interpreting the triangles $\mathbf{p}_i\mathbf{p}_{i+1}\mathbf{P}$ as quads with one edge collapsed to $\mathbf{P}$ enables a conversion to a partial BB-net with coefficients $\hat{\mathbf{b}}^r_{i,j}$, $i = 0,\dots,3$, $j = 0,\dots,2$ (green in Fig. 11a). Degree raising to 4 in the radial direction yields three layers of BB-coefficients $\mathbf{b}^r_{ij}$ of the cap outside the red central point and tangent layer, see Fig. 11b. The first-order expansion of the degree (3,4) cap at the pole is defined by setting $\mathbf{C}$ as the limit point of bi-3 polar subdivision B3PS

$$\mathbf{C} := \frac{2}{3}\mathbf{P} + \frac{1}{3m}\sum_{i=0}^{m-1}\mathbf{p}_i, \tag{7}$$

and defining the tangent plane as the linear image of a regular m-gon

$$\mathbf{b}^i_{03} := \mathbf{C} + \frac{2}{m}\sum_{s=0}^{m-1} \mathsf{c}_s \frac{\mathbf{C} + 3\hat{\mathbf{b}}^{i+s}_{02}}{4}, \quad \mathbf{b}^{i-1}_{33} := \mathbf{b}^i_{03}. \tag{8}$$

The points $\mathbf{b}^i_{03}$, $\mathbf{b}^i_{33}$ and $\mathbf{C}$ define a polar parameterized plane and hence

$$\mathbf{b}^i_{13} := \frac{2\mathbf{b}^i_{03} + \mathbf{b}^i_{33}}{\mathsf{c}+2} + \frac{\mathsf{c}-1}{\mathsf{c}+2}\mathbf{C}, \qquad \mathbf{b}^i_{23} := \frac{2\mathbf{b}^i_{33} + \mathbf{b}^i_{03}}{\mathsf{c}+2} + \frac{\mathsf{c}-1}{\mathsf{c}+2}\mathbf{C}. \tag{9}$$

The resulting cap is C^2-connected to the surrounding surface, internally C^2 and C^1 at the pole.

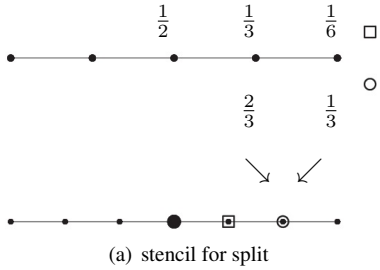

(a) stencil for split

Figure 12: Transformation of a degree 4 curve into two C^2-connected cubics with the stencils above for □ and below for ○.

Bi-3 macropatches. Applying the stencils of Fig. 12 symetrically and setting the common coefficient ● as a the average of its neighbors creates C^2 layer curves to replace the degree 4 layer curves of the degree (3,4) cap. The result is a $2m$ piece bi-3 polar cap that essentially preserves the highlight line distribution of the degree (3,4) cap, joins C^2 with the surrounding surface and is internally C^2 except at the pole where it is C^1.

5.1. Refinement in the vicinity of polar configurations

Refinement can be used to add detail as illustrated in Fig. 16, or to separate *tight configurations* where multiple irregular nodes or facets are in close proximity. The challenge is to refine without harming the highlight line distribution near the pole.

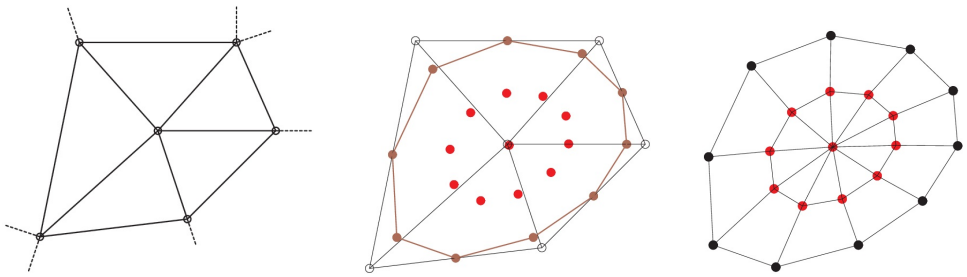

(a) (b) (c)

Figure 13: Preprocessing in tight configurations. (a) Tight polar input. (b) Refinement in circulant direction followed by B3PS refinement. (c) The • were defined by the surrounding input mesh.

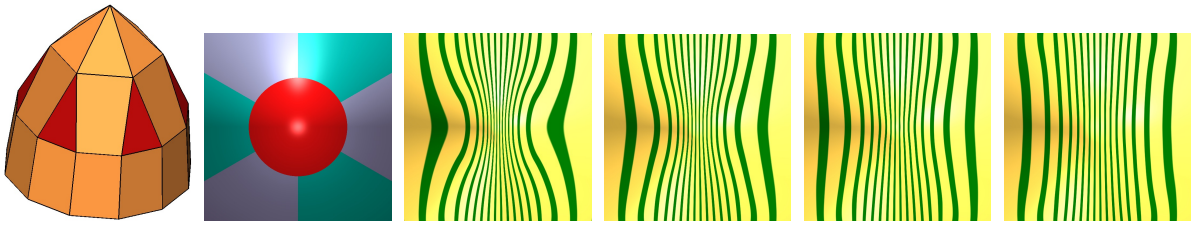

(a) layout (b) naive1 (c) naive2 (d) naive3 (e) default

Figure 14: Comparison of bi-3 generalizing constructions for conical input. Rejected options and default with highlight lines.

Single refinement in tight configurations. When the direct neighbor of the polar node is part of a T-gon (see Fig. 18a,e) or if it has valence $n \neq 4$ (see Fig. 19a) then the earlier cap construction is not well-defined. We proceed as follows.

- Interpret the ring of neighbors of the polar node as the control polygon of a cubic uniform spline in B-spline form and double the number control points by uniform knot insertion. In Fig. 13b, ∘ indicate original and • indicate (auxiliary) refined nodes.
- Derive new • in Fig. 13b by applying the B3PS-refinement rules to • and the initial polar node.
- Replace the auxiliary nodes • by the nodes • (see Fig. 13c) generated as a refinement to accommodate G-splines or GT-splines as in Karčiauskas and Peters (2019a).

Here the second ring of neighbors of the polar node (dashed in Fig. 1a) influences • and hence the shape of the polar cap and the entirety of • affect the refined nets used for construction of surfaces abutting the polar cap. Fortunately this interplay is well balanced and results in a good highlight line distribution.

Fig. 14 compares the construction to alternative, at a first glance natural, pre-processing refinements that result in visible artifacts compared to the above *default* option. For example, treating the polar triangles as quads with a collapsed edge, the nodes $\bullet^{GT(3)}$ and $\bullet^{GT(3)}$ resulting from GT(3) τ-gon refinement can be taken in lieu of the • and • nodes of Fig. 13b; and the polar node defined as (option: naive1) the initial polar node $\mathbf{P}^0$ or as (option: naive2) the weighted average $(7\mathbf{P}^0 + \mathbf{A})/8$, where $\mathbf{A}$ is the average of the $\bullet^{GT(3)}$ and the ratio 7:1 gives the best visual result. A third option is to combine $\bullet^{GT(3)}$ and • of the default algorithm. Complementing C^2 bi-3 surfaces, interrogation with highlight lines reveals that the default is best; 'naive3' is almost as good but has less desirable, more 'pinched' highlight lines. 'naive1' corresponds to a more pointed cap. One explanation for the pinching artifacts is that interpreting the polar triangles as degenerate quads pulls the mesh too much towards the pole. The default slows this movement.

Refinement for analysis. The above refinement serves well to add regular nodes and preserve good shape, but does not express the original surface in terms of more degrees of freedom as is required for engineering analysis theory. An analysis-friendly, reproducing refinement is derived in two steps.

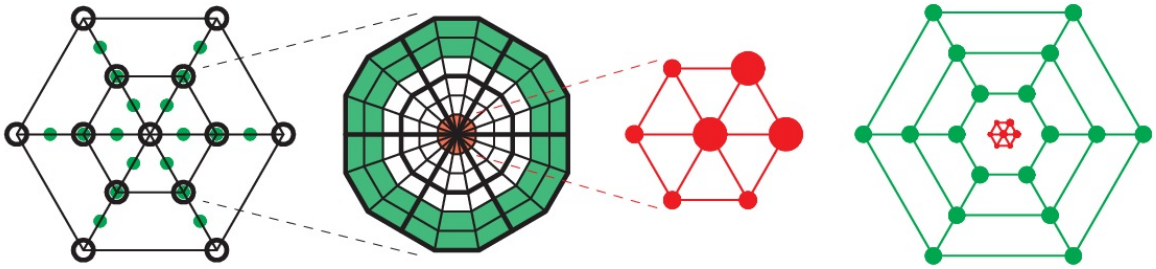

(a) input polar control net bi-3 cap new control net

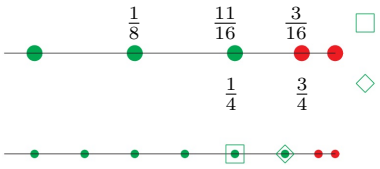

(b) refinement stencil

Figure 15: Refinement of the bi-3 cap.

First, the polar net (whose nodes are circles in Fig. 15a) is transformed by

- doubling the number of • control points by radial uniform cubic subdivision. This yields the layers of green-underlaid BB-coefficients of the bi-3 cap in Fig. 15a and ensures C^2 connection to the surrounding surface.
- The three enlarged large central coefficients define, by the recurrence (4), the remaining central control nodes marked •. The central nodes are converted to BB-form via (3). This defines red-underlaid BB-coefficients at the center of the bi-3 cap, Fig. 15a.
- The BB-coefficients between the green circular layers $\mathbf{b}$ and the red circular layers $\tilde{\mathbf{b}}$ are set so that radial layers are C^2:

$$\mathbf{b}_3 := \mathbf{b}_2 + \frac{1}{4}(\tilde{\mathbf{b}}_2 - \mathbf{b}_1), \quad \tilde{\mathbf{b}}_0 := \mathbf{b}_3, \quad \tilde{\mathbf{b}}_1 := \mathbf{b}_2 + \frac{1}{2}(\tilde{\mathbf{b}}_2 - \mathbf{b}_1). \tag{10}$$

Second, the new net is refined radially, then circularly. The bullets of the *top* row of Fig. 15b represent a typical radial layer, with the rightmost • the pole.

- The coefficients marked • in the *bottom* row are obtained from *top* • by knot insertion. The formulas for the coefficients additionally marked by a hollow box and a diamond are given by the stencils above and below the top line segment.
- The rightmost • (bottom line) representing the pole remains stationary; its neighbor, marked as • is the average of the pole and its neighbor (top line segment).
- Apply knot insertion to the circular C^2 layers.

Recall that only three nodes (enlarged, red in Fig. 15) can be set independently.

5.2. *Visual comparison*

As in Section 4, we extend a net used for construction of the polar cap by an additional layer of nodes in Fig. 17a to generate a surrounding strip of regular bi-3 patches (green in Fig. 17e) and so assess the transition to the polar cap.

The difference between everywhere C^2 bi-65 surfaces (reviewed in the Appendix) and C^2 bi-3 surfaces that are only C^1 at the pole is best visible in the curvature distribution, see Fig. 17. The C^2 bi-3 splines represent a remarkable improvement over the analogous surfaces in Fig. 8.

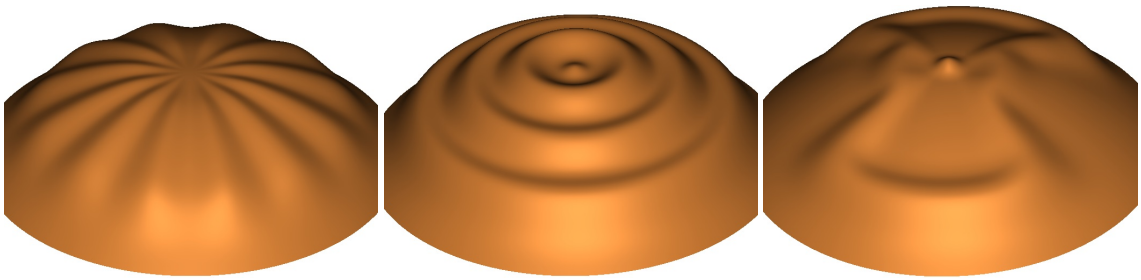

Figure 16: Using refinement to add detail to the bi-3 polar cap of Fig. 2c.

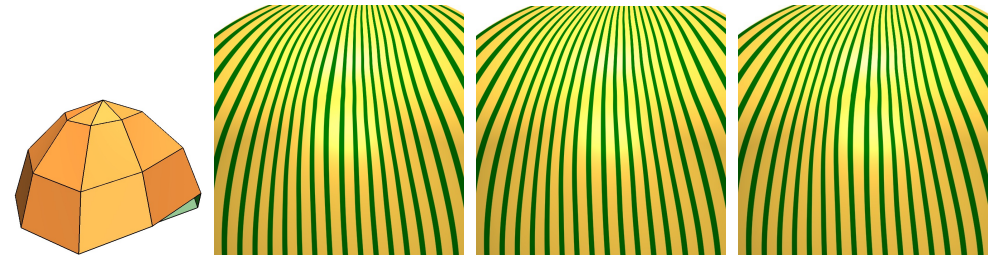

(a) net, $m = 8$ (b) bi-34 (c) bi-65 (d) bi-3

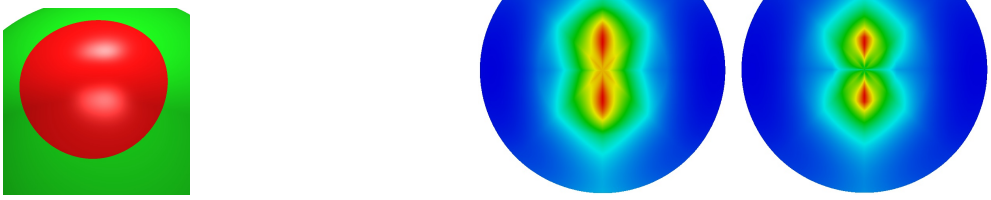

(e) layout (g) bi-65 Gauss (h) bi-3 Gauss

Figure 17: Comparing bi-3 generalizing constructions for an extended convex polar net with oscillating base line. Highlight lines and Gauss curvature attest to high quality of the purely bi-3 cap.

All surfaces in Fig. 18 are bi-3. This means that the GT-splines for overlapping τ_1-configurations formally join only C^0. Yet this lack of formal smoothness is not visible – also in considerably harder configurations.

Fig. 19 illustrates the treatment of irregular configurations in close proximity: nodes with $n \neq 4$ neighbors, τ-configurations and polar configurations combine to form one semi-structured spline modeling the whole surface.

6. Conclusion

Polar caps can close off a large variety of tube-like surfaces without introducing shape artifacts. Their control net consists of a cone of m triangles and the surface consists of a small multiple of m polynomial pieces. Tight configurations, where vertices of the control net belong to other semi-regular structures, admit polar caps after a local refinement. The quality of the caps is consistent or better than that of the underlying regular spline: lower for bi-2 C^1 splines and higher for bi-3 C^2 splines. G^1 polar caps of degree as low as $(3, 4)$ and $(3, 3)$ deliver high-quality highlight line distributions, that are on par with a high-end degree 6,5 G^2 construction (see Appendix) but with simpler algorithms.

Acknowledgements. This work was supported in part by DARPA HR00111720031 and NIH R01 EB018625.

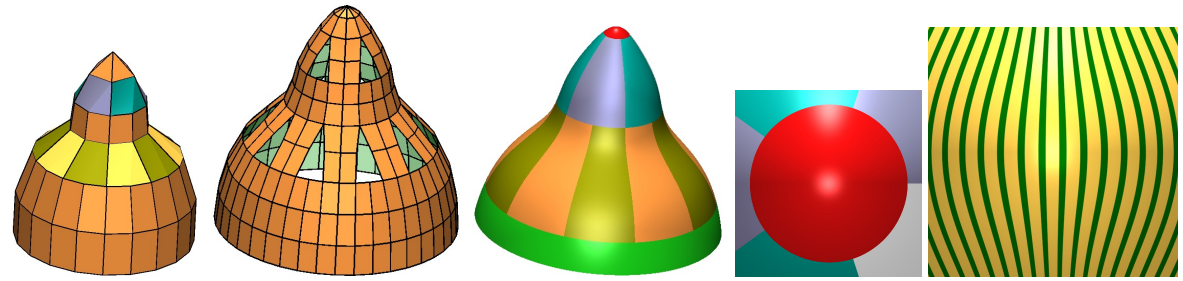

(a) polar valence 5 (b) refined mesh (c) surface (d) polar vicinity of Fig. 18c

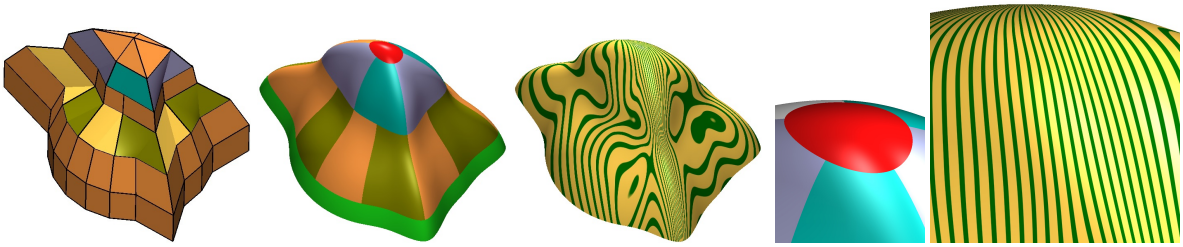

(e) perturbation of Fig. 18a (f) polar vicinity after perturbation

Figure 18: Meshes with tightly packed T_1-gons and completed with polar configuration (a,e). (b) Refinement to form a unified net. This succeeds also for adjacent T_1-gons. The polar configuration is refined to an overall consistent refined mesh. (c,e) Layout of resulting bi-3 surface; the regular bi-3 patches form a bottom green strip, a polar cap is displayed as a top red disk. (d,f) The highlight line distribution of the polar cap.

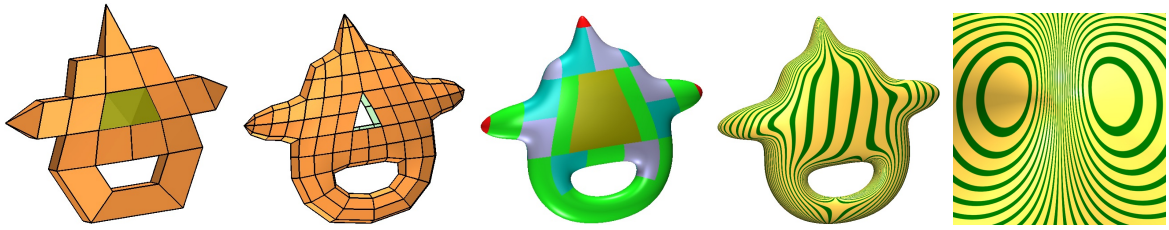

(a) mesh (b) refinement (c) layout (d) highlights (e) vicinity of top cap

Figure 19: Tight 'bottle opener' mesh. The top pole node is a direct neighbor of nodes of valence 5. Bi-3 polar caps, n-sided surface pieces (blue and gray) and T-junctions all generalize bi-3 splines in the regular parts of the semi-structured control net.

References

Catmull, E., Clark, J., 1978. Recursively generated B-spline surfaces on arbitrary topological meshes. Computer-Aided Design 10, 350–355.

DeRose, T.D., 1990. Necessary and sufficient conditions for tangent plane continuity of Bézier surfaces. Comp Aid Geom Design 7, 165–179.

Farin, G., 1988. Curves and Surfaces for Computer Aided Geometric Design: A Practical Guide. Academic Press.

Gregory, J.A., Hahn, J.M., 1987. Geometric continuity and convex combination patches. Computer Aided Geometric Design 4, 79–89.

Groisser, D., Peters, J., 2015. Matched G^k-constructions always yield C^k-continuous isogeometric elements. Computer Aided Geometric Design 34, 67–72.

Karčiauskas, K., Myles, A., Peters, J., 2006. A C^2 polar jet subdivision, in: Scheffer, A., Polthier, K. (Eds.), Proceedings of Symposium of Graphics Processing (SGP), June 26-28 2006, Cagliari, Italy, ACM Press. pp. 173–180.

Karčiauskas, K., Peters, J., 2007. Bicubic polar subdivision. ACM Trans. Graph. 26, 14.

Karčiauskas, K., Peters, J., 2009. Finite curvature continuous polar patchworks, in: Hancock, E., Martin, R., Sabin, M. (Eds.), IMA Mathematics of Surfaces XIII Conference, pp. 222–234.

Karčiauskas, K., Peters, J., 2015a. Point-augmented biquadratic C^1 subdivision surfaces. Graphical Models 77, 18–26.

Karčiauskas, K., Peters, J., 2015b. Smooth multi-sided blending of biquadratic splines. Computers & Graphics 46, 172–185.

Karčiauskas, K., Peters, J., 2019a. High quality refinable G-splines for locally quad-dominant meshes with T-gons. Computer Graphics Forum 38, 151–161.

Karčiauskas, K., Peters, J., 2019b. Refinable smooth surfaces for locally quad-dominant meshes with T-gons. Computers& Graphics 82, 193–202.

Loop, C.T., Schaefer, S., 2008. G ^{2} tensor product splines over extraordinary vertices. Comput. Graph. Forum 27, 1373–1382.

Myles, A., Karčiauskas, K., Peters, J., 2008. Pairs of bi-cubic surface constructions supporting polar connectivity. Comput. Aided Geom. Des. 25, 621–630. doi:http://dx.doi.org/10.1016/j.cagd.2008.06.002.
Myles, A., Peters, J., 2009. Bi-3 C^2 polar subdivision. ACM Transactions on Graphics 28. Siggraph 2009.
Myles, A., Peters, J., 2011. C^2 splines covering polar configurations. Computer Aided Design 43, 1322–1329.
Shi, K.L., Yong, J.H., Sun, J.G., Paul, J.C., 2010. Gn blending multiple surfaces in polar coordinates. Computer-Aided Design 42, 479–494.
Shi, K.L., Yong, J.H., Tang, L., Sun, J.G., Paul, J.C., 2013. Polar NURBS surface with curvature continuity. Computer Graphics Forum 32, 363–370.
Toshniwal, D., Speleers, H., Hiemstra, R., Hughes, T., 2017. Multi-degree smooth polar splines: A framework for geometric modeling and isogeometric analysis. Computer Methods in Applied Mechanics and Engineering 316, 1005–1061.
Várady, T., Salvi, P., Rockwood, A.P., 2012. Transfinite surface interpolation with interior control. Graphical Models 74, 311–320.
Wang, J., Cheng, F., 2013. Polar embedded catmull-clark subdivision surface, in: CAD/Graphics, IEEE. pp. 24–31.
Wang, J., Cheng, F., 2016. G2 interpolation for polar surfaces. Computer-Aided Design and Applications 13, 610–617.

Appendix: A polar G^2 cap of degree (6,5)

To ensure that the low-degree constructions of Section 5 have highlight line distributions comparable to curvature continuous constructions, we devised an algorithm that differs from the G^2 construction of Karčiauskas and Peters (2009) only in an improvement of the central quadratic expansion $\mathbf{q}$ and preserves its highlight lines and curvature images. Since the improvement simplifies the original, it is presented here for readers who want to implement and compare themselves a G^2 construction to the algorithms of this paper.

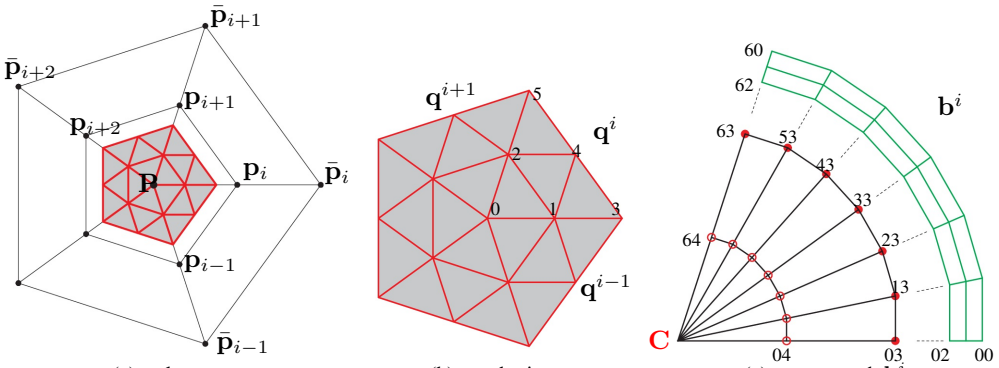

(a) polar net (b) quadratic $\mathbf{q}$ (c) sector patch $\mathbf{b}^i$

Figure 20: Degree $(6, 5)$ construction. Notations for polar net as in Fig. 11a.

The central point $\mathbf{q}^i_0 := \mathbf{C}$ of the quadratic expansion is set to the limit point of bi-3 polar subdivision B3PS (7).

Then for $i = 0, \dots, m-1$, (see Fig. 20a,b)

$$\begin{aligned}
\mathbf{q}_1^i :=& \mathbf{C} + w \sum_{s=0}^{m-1} \mathsf{c}_s \mathbf{p}_{i+s} + \bar{w} \sum_{s=0}^{m-1} \mathsf{c}_s \bar{\mathbf{p}}_{i+s}, \quad \mathbf{q}_2^{i-1} := \mathbf{q}_1^i; \\
\mathbf{q}_3^i :=& (1 - w_0' - \bar{w'}_0)\mathbf{P} + \frac{w_0'}{m} \sum_{s=0}^{m-1} \mathbf{p}_s + \frac{\bar{w'}_0}{m} \sum_{s=0}^{m-1} \bar{\mathbf{p}}_s + w_1' \sum_{s=0}^{m-1} \mathsf{c}_s \mathbf{p}_{i+s} \\
&+ w_2' \sum_{s=0}^{m-1} \mathsf{c}_{2s} \mathbf{p}_{i+s} + \bar{w'}_1 \sum_{s=0}^{m-1} \mathsf{c}_s \bar{\mathbf{p}}_{i+s} + \bar{w'}_2 \sum_{s=0}^{m-1} \mathsf{c}_{2s} \bar{\mathbf{p}}_{i+s}, \quad \mathbf{q}_5^{i-1} := \mathbf{q}_3^i; \\
\mathbf{q}_4^i :=& (1 - w_0'' - \bar{w''}_0)\mathbf{P} + \frac{w_0''}{m} \sum_{s=0}^{m-1} \mathbf{p}_s + \frac{\bar{w''}_0}{m} \sum_{s=0}^{m-1} \bar{\mathbf{p}}_s \\
&+ w_1'' \sum_{s=0}^{m-1} \mathsf{c}_s \frac{\mathbf{p}_{i+s} + \mathbf{p}_{i+s+1}}{2} + w_2'' \sum_{s=0}^{m-1} \mathsf{c}_{2s} \frac{\mathbf{p}_{i+s} + \mathbf{p}_{i+s+1}}{2} \\
&+ \bar{w''}_1 \sum_{s=0}^{m-1} \mathsf{c}_s \frac{\bar{\mathbf{p}}_{i+s} + \bar{\mathbf{p}}_{i+s+1}}{2} + \bar{w''}_2 \sum_{s=0}^{m-1} \mathsf{c}_{2s} \frac{\bar{\mathbf{p}}_{i+s} + \bar{\mathbf{p}}_{i+s+1}}{2}.
\end{aligned} \tag{11}$$

The following proposition can be checked by substitution.

Proposition 1. *If*

$$\begin{aligned}
&w_1' := 2w, \ \bar{w'}_1 := 2\bar{w}, \\
&w_0'' := \mathsf{c} w_0' + \frac{1-\mathsf{c}}{3}, \ \bar{w''}_0 := \mathsf{c}\bar{w'}_0, \quad w_1'' := 2w, \ \bar{w''}_1 := 2\bar{w}, \quad w_2'' := \frac{w_2'}{\mathsf{c}}, \ \bar{w''}_2 := \frac{\bar{w'}_2}{\mathsf{c}},
\end{aligned}$$

then $\mathbf{q}^i$ *and* $\mathbf{q}^{i+1}$ *are* C^2 *connected.*

Corollary 1. *The pieces* $\mathbf{q}^i$ *are part of a single* C^2 *quadratic expansion.*

It remains to choose w, $\bar{w}$, w_0', $\bar{w'}_0$, w_2', $\bar{w'}_2$ to optimize shape and simplify the implementation. Good shape is achieved for

$$\bar{w} := 0, \quad w_0' := \frac{10}{9}, \quad \bar{w'}_0 := \frac{1}{18}, \quad \bar{w'}_2 := \frac{w_2'}{34}, \tag{12}$$

and, for even $m \le 20$,

m =	6	8	10	12	14	16	18	20
w :=	0.139	0.112	0.093	0.079	0.069	0.06	0.054	0.049
w_2' :=	0.315	0.315	0.29	0.262	0.235	0.213	0.193	0.176

For odd $m = 7, \dots, 19$, the parameters are interpolated: $w(2s{+}1) := \frac{w(2s)+w(2s+2)}{2}$, $w_2'(2s{+}1) := \frac{w_2'(2s)+w_2'(2s+2)}{2}$. And for $m > 20$,

$$w(m) := \frac{0.00079m + 0.96939}{m}, \ w_2'(m) := \frac{0.01158m + 3.3274}{m}.$$

Finally, knot insertion in circular direction doubles the valences of $m = 3, 4, 5$ and so reduces these cases to $m = 6, 8, 10$. This completes the construction of the quadratic expansion $\mathbf{q}$.

The BB-coefficients $\mathbf{b}_{sr}^i$ of bi-65 patch (see Fig. 20c) are then defined as follows. Conversion to a partial BB-net as in Section 5 and degree-raising to $(6, 5)$ yields the green layers $\mathbf{b}_{rs}^i$, $r = 0, \dots, 6$, $s = 0, 1, 2$. At the pole $\mathbf{b}_{r5}^i := \mathbf{C}$,

layer 4 is defined by degree-raising to 6 the cubic defined by formulas (9), $\mathbf{b}^i_{04} := \frac{3}{5}\mathbf{q}^i_0 + \frac{2}{5}\mathbf{q}^i_1$ and $\mathbf{b}^i_{64} := \frac{3}{5}\mathbf{q}^i_0 + \frac{2}{5}\mathbf{q}^i_2$. We set

$$\begin{aligned}
\mathbf{b}^i_{03} :=& \frac{1}{10}\big(3\mathbf{q}^i_0 + 6\mathbf{q}^i_1 + \mathbf{q}^i_3\big),\\
\mathbf{b}^i_{13} :=& \frac{1}{10(2+\mathsf{c})}\big((3+6\mathsf{c})\mathbf{q}^i_0 + (11+4\mathsf{c})\mathbf{q}^i_1 + 3\mathbf{q}^i_2 + 2\mathbf{q}^i_3 + \mathbf{q}^i_4\big),\\
\mathbf{b}^i_{23} :=& \frac{1}{50(2+\mathsf{c})^2}\big((15+78\mathsf{c}+42\mathsf{c}^2)\mathbf{q}^i_0 + (92+80\mathsf{c}+8\mathsf{c}^2)\mathbf{q}^i_1 + (54+36\mathsf{c})\mathbf{q}^i_2\\
&+ (16+2\mathsf{c})\mathbf{q}^i_3 + (20+4\mathsf{c})\mathbf{q}^i_4 + 3\mathbf{q}^i_5\big),\\
\mathbf{b}^i_{33} :=& \frac{1}{100(2+\mathsf{c})^2}\big(3(7+52\mathsf{c}+31\mathsf{c}^2)\mathbf{q}^i_0 + 3(49+40\mathsf{c}+\mathsf{c}^2)(\mathbf{q}^i_1 + \mathbf{q}^i_2)\\
&+ 18(\mathbf{q}^i_3 + \mathbf{q}^i_5) + (49+4\mathsf{c}+\mathsf{c}^2)\mathbf{q}^i_4\big),
\end{aligned}$$

and the remaining BB-coefficients $\mathbf{b}^i_{43}$, $\mathbf{b}^i_{53}$, $\mathbf{b}^i_{63}$ are defined by symmetry.

Fig. 21 compares the C^2 degree (6,5) cap to the bi-3 cap of Section 5 for convex and wavy meshes. The highlight line distributions are near indistinguishable ((b) vs (c)) unless one looks directly from the top where the bi-3 shape is not quite as uniform; the second row, (i) vs (j) confirms a slightly more pointed bi-3 cap whereas the (6,5) construction spreads out more due to its quadratic expansion.

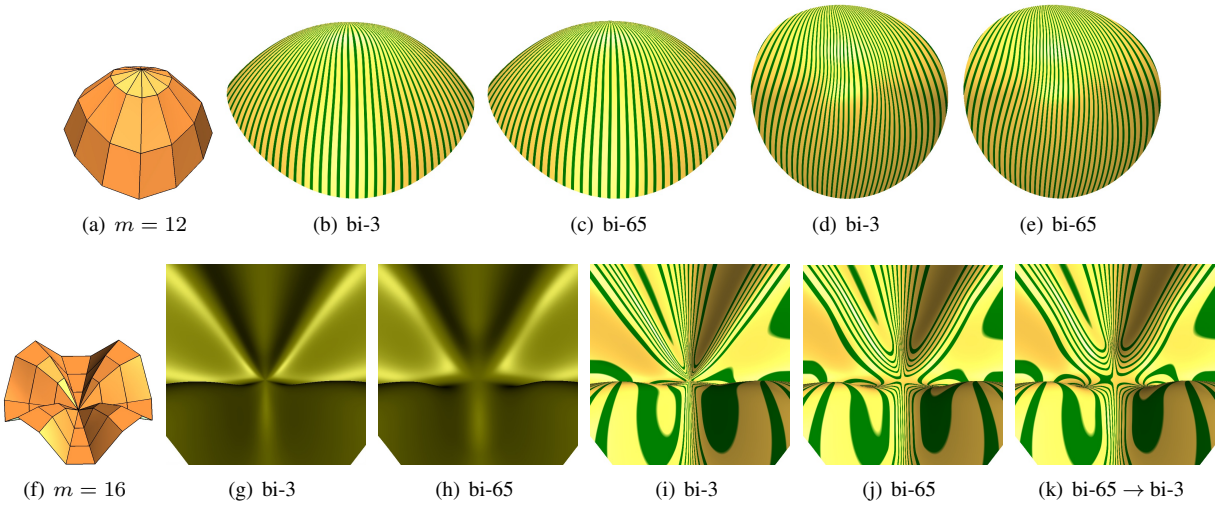

(a) $m = 12$ (b) bi-3 (c) bi-65 (d) bi-3 (e) bi-65

(f) $m = 16$ (g) bi-3 (h) bi-65 (i) bi-3 (j) bi-65 (k) bi-65 → bi-3

Figure 21: Comparison of bi-3 and bi-65 constructions: *top* convex net, $m = 12$; *bottom* wavy net, $m = 16$.

Using the (6,5) patch as a guide, we can construct a bi-3 polar cap alternative to Section 5 as m 3-piece C^2 bi-3 macro-patches. Observing that the layers $\mathbf{b}^i_{rj}$, $j = 0, 1, 2, 4$ are of actual degree 3 we can transform layer 3 to degree 3 by defining B-spline control points $\mathbf{d}^i := -4\mathbf{b}^i_{03} + 10\mathbf{b}^i_{13} - 5\mathbf{b}^i_{23}$. By matching the second-order Hermite data at either end, each radial layer of degree 5 is approximated by three uniquely determined C^2-connected segments. Fig. 21k illustrates that a good highlight line distribution can be achieved by the guided approach despite the low degree.